J Stat Phys (2016) 162:232–241
DOI 10.1007/s10955-015-1387-6

Elasticity of Random Multiphase Materials: Percolation of the Stiffness Tensor

Ying Chen[1] · **Christopher A. Schuh**[2]

Received: 5 May 2015 / Accepted: 30 September 2015 / Published online: 15 October 2015

Abstract Topology and percolation effects play an important role in heterogeneous materials, but have rarely been studied for higher-order tensor properties. We explore the effective elastic properties of random multiphase materials using a combination of continuum computational simulations and analytical theories. The effective shear and bulk moduli of a class of symmetric-cell random composites with high phase contrasts are determined, and reveal shortcomings of classical homogenization theories in predicting elastic properties of percolating systems. The effective shear modulus exhibits typical percolation behavior, but with its percolation threshold shifting with the contrast in phase bulk moduli. On the contrary, the effective bulk modulus does not exhibit intrinsic percolation but does show an apparent or extrinsic percolation transition due to cross effects between shear and bulk moduli. We also propose an empirical approach for bridging percolation and homogenization theories and predicting the effective shear and bulk moduli in a manner consistent with the simulations.

Keywords Percolation · Homogenization theory · Elastic theory · Effective elastic moduli · Random multiphase materials · Composite materials

Predicting the effective elastic properties of heterogeneous materials is a fundamental interdisciplinary problem in physics, materials, and mechanics due to the pervasive presence of random multiphase materials in nature and engineering [1,2]. Many composite homogenization theories for effective elastic properties have quantitatively incorporated the effects of phase geometry and anisotropy, but largely overlook the role of disorder, topology, and per-

✉ Ying Chen
cheny20@rpi.edu

[1] Department of Materials Science and Engineering, Rensselaer Polytechnic Institute, 110 8th Street, Troy, NY 12180, USA

[2] Department of Materials Science and Engineering, Massachusetts Institute of Technology, 77 Massachusetts Avenue, Cambridge, MA 02139, USA

colation [3–5]. On the other hand, the percolation community has explored elastic rigidity percolation [6–11] and coupled diffusion-force percolation [12,13] on random networks or lattices as well as the concept of "continuum percolation" [14–20], which deals with topological percolation effects in multiphase solids. However, existing studies on percolation are mostly limited to isotropic linear transport properties where the second-order transport coefficient tensor for each phase reduces to a scalar [21–23]. Studies on continuum percolation also tend to estimate effective properties by mapping the continuum to a discrete lattice [24–27], which is now known to produce artifacts as compared to a true continuum response [28]. Elucidating percolation effects in elasticity and incorporating them in continuum homogenization theories could significantly advance mesoscale predictive capabilities that connect heterogeneous microstructures to macroscopic properties. In this paper, we establish the effective elastic properties of random multiphase materials by continuum calculations that quantitatively capture topology and percolation effects, and also demonstrate the deficiencies of classical homogenization theories when applied to percolating systems. We further examine an approach that bridges percolation and homogenization theories and elucidates the observed disparate percolation behavior in bulk and shear moduli.

Our model system is a two-dimensional square domain containing 12766 cells from hexagonal tessellations. Each cell is randomly assigned a phase identity (either phase 1 or phase 2) with a desired probability, and inter-phase boundaries are assumed to be perfect interfaces with continuity of field variables required across them. This model system belongs to a class of materials widely known as "symmetric-cell materials" [4]. Each phase is described by a stiffness tensor C that relates strain ε to stress σ via Hooke's law: $\sigma_{ij} = C_{ijkl}\varepsilon_{kl}$. Under the assumption of isotropy, there are two independent elastic constants in C, e.g., the bulk modulus K and the shear modulus G.

$$\sigma_{ij} = K\delta_{ij}\varepsilon_{kk} + 2G\varepsilon'_{ij} \tag{1}$$

where ε_{kk} is the volumetric strain, ε'_{ij} is the deviatoric strain, and δ_{ij} is the Kronecker delta. Under the plane strain condition that is applied to the system, the indices i, j, k can be 1 or 2, and K differs from its three-dimensional counterpart while G remains the same. We impose an orthogonal mixed boundary condition (where displacements are applied on all sides of the specimen without friction), as the static (uniform traction) and kinematic (uniform displacement) conditions usually lead to a lower and upper bound for the effective elastic properties [29,30]. Finite element calculations are carried out using quadratic triangular elements and an adaptive re-meshing technique that yields finer meshes at high stress locations, to ensure a reliable and sufficiently resolved continuum solution for the stress and strain fields; the mesh size is therefore generally much smaller than the phase domain size. The effective plane strain bulk and shear moduli, K_{eff} and G_{eff}, are defined through

$$\langle\sigma_{ij}\rangle = K_{eff}\delta_{ij}\langle\varepsilon_{kk}\rangle + 2G_{eff}\langle\varepsilon'_{ij}\rangle \tag{2}$$

where $<>$ denotes an average over the entire sample.

We start with a simple case where the two phases have equal bulk moduli ($K_1 = K_2 = K = 6.25 \times 10^6$) but different shear moduli ($G_1 = 5 \times 10^2$, $G_2 = 5 \times 10^6$). The units for all moduli and stresses are the same (and are arbitrary). As shown in Fig. 1a, the effective shear modulus G_{eff} increases nonlinearly with the fraction of phase 2, p. The simulation results lie between the widely-separated, rigorous Hashin lower and upper bounds for effective shear modulus of isotropic composites (drawn as blue dashed lines) [31].

$$G^{(-)} = G_1 + \frac{p}{\frac{1}{G_2 - G_1} + \frac{(1-p)(K_1+2G_1)}{2G_1(K_1+G_1)}} \tag{3}$$

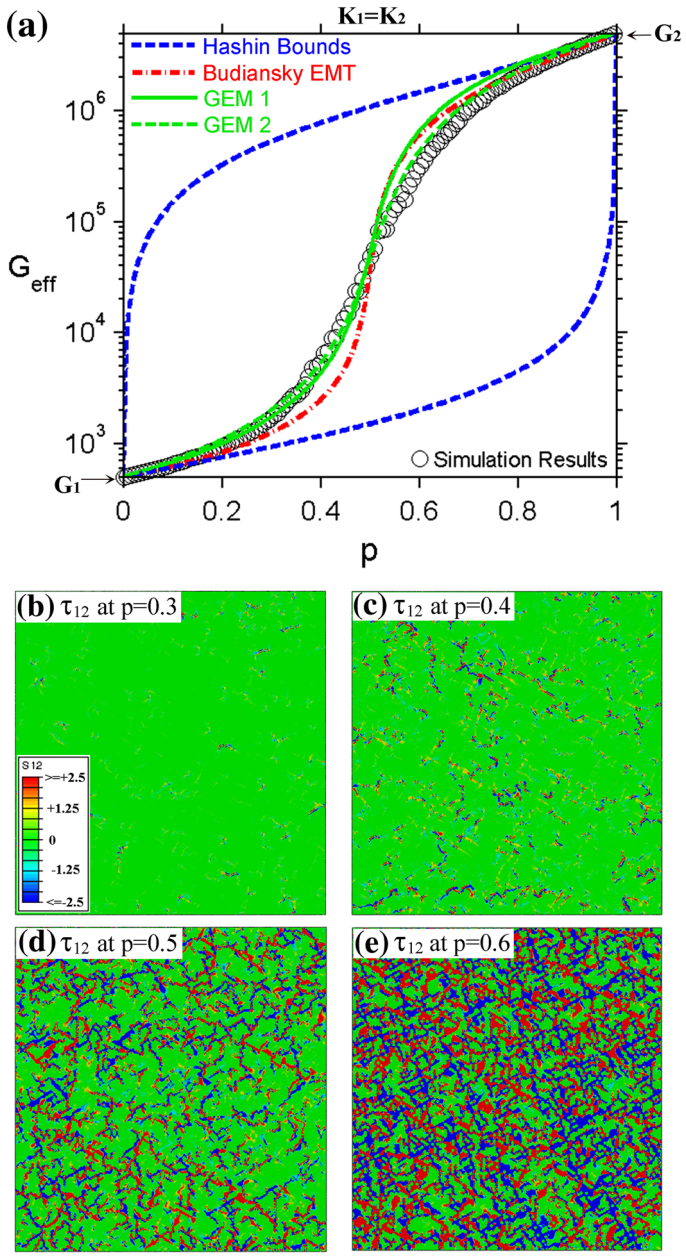

Fig. 1 (Color online) **a** The effective shear modulus G_{eff} when the two phases have equal bulk moduli ($K_1 = K_2 = 6.25 \times 10^6$) but different shear moduli ($G_1 = 5 \times 10^2$ and $G_2 = 5 \times 10^6$) as a function of the volume fraction p of phase 2. The *blue dashed lines* are the Hashin lower and upper bounds for G_{eff} [Eqs. (3–4)]. The *red dash-dot line* shows the predictions from the Budiansky EMT equation [Eq. (5)]. The two *green solid lines* result from the GEM equation [Eq. (6)] using two sets of scaling exponents. **b–e** The distribution of shear stress τ_{12} at different phase fractions, showing the development of percolative stress paths with increasing phase fraction p.

$$G^{(+)} = G_2 + \frac{1-p}{\frac{1}{G_1-G_2} + \frac{p(K_2+2G_2)}{2G_2(K_2+G_2)}} \tag{4}$$

Figure 1a also compares the simulation results with Budiansky effective medium theory (EMT) for G_{eff} [32], which was derived based on the assumption that each particle is embedded in an effective medium and can be described by the Eshelby solution [33].

$$(1-p)\frac{G_1 - G_{eff}}{G_1 + (\beta^{-1}-1)G_{eff}} + p\frac{G_2 - G_{eff}}{G_2 + (\beta^{-1}-1)G_{eff}} = 0 \tag{5}$$

where the strain proportionality parameter $\beta = (6K + 10G_{eff})/(15K + 15G_{eff})$ in three dimensions and $(3K + 5G_{eff})/(6K + 4G_{eff})$ in two dimensions for the case of $K_1 = K_2 = K$. Predictions from Eq. (5) were lower than the simulation results when $p < 0.5$ but overshoot at higher p.

Equation (5) implicitly assumes a percolation threshold at $p_c = \beta$ (regardless of phase geometry and topology), which is dependent on phase bulk moduli and is approximately 3/6 = 0.5 in the present two dimensional case (as $K > G_2 \gg G_1$ and therefore $K \gg G_{eff}$). Equation (5) also tacitly assumes scaling exponents of unity around the percolation threshold. These implicit assumptions are made clear by comparison with the so-called generalized effective medium (GEM) equation [34,35], which is a semi-empirical mixing rule that conforms to the well-known power-law scalings of percolation theory near the threshold:

$$(1-p)\frac{G_1^{1/s} - G_{eff}^{1/s}}{G_1^{1/s} + (p_c^{-1}-1)G_{eff}^{1/s}} + p\frac{G_2^{1/t} - G_{eff}^{1/t}}{G_2^{1/t} + (p_c^{-1}-1)G_{eff}^{1/t}} = 0 \tag{6}$$

The GEM equation Eq. (6) incorporates the percolation threshold p_c in the same position as β from Eq. (5). It also incorporates the percolation scaling exponents s and t, and implicitly captures the coupling between K and G_{eff} through p_c and possibly s and t.

In the present elasticity problem, the relevant percolation threshold and scaling exponents are not known a priori, so we proceed by fitting the data as follows. Considering $G_{eff} \geq \sqrt{G_1 G_2}$ as "percolating" (percolation probability is one) and otherwise "not percolating" (percolation probability is zero), the average percolation probability Π at a certain phase fraction p can be evaluated by averaging over the percolation probability of many simulations run at this p value. The square root property product ($\sqrt{G_1 G_2}$) is chosen for its special significance in percolation theory, being derived from phase-interchange or duality relations [1,4]. We thus obtain the average percolation probability $\Pi(p)$ from our data and define p_c as the phase fraction corresponding to $\Pi = 0.5$ (see the inset in Fig. 3a showing Π as a function of p) [36]. p_c is found to be ~0.503, which happens to be similar to the geometric connectivity or conductivity percolation threshold of 0.5 for the present hexagonal cell geometry (i.e., for site percolation on its dual, triangular lattice) [36]. Subsequently, fitting Eq. (7)

$$G_{eff}(p) \propto \begin{cases} (p_c - p)^{-s} & \text{for} \quad p < p_c \\ (p - p_c)^{t} & \text{for} \quad p > p_c \end{cases} \tag{7}$$

to simulation data on the range $|p - p_c| \leq 0.12$ leads to $s \approx 1.38$, $t \approx 1.26$, both of which happen to be similar to $s = t = 1.3$ for conductivity problems [37]. Predictions from Eq. (6) using the extracted p_c, s, and t values, plotted as the green solid line in Fig. 1a, are close to simulation data although slightly underestimate below p_c and overestimate above p_c. Fitting Eq. (7) to a much broader range of simulation data ($|p - p_c| \leq 0.4$) results in $s \approx 1.55$ and $t \approx 1.55$ (which are no longer percolation scaling exponents, strictly speaking), and using them in Eq. (6) leads to a slightly better fit (green dashed line in Fig. 1a). Figure 1b–e

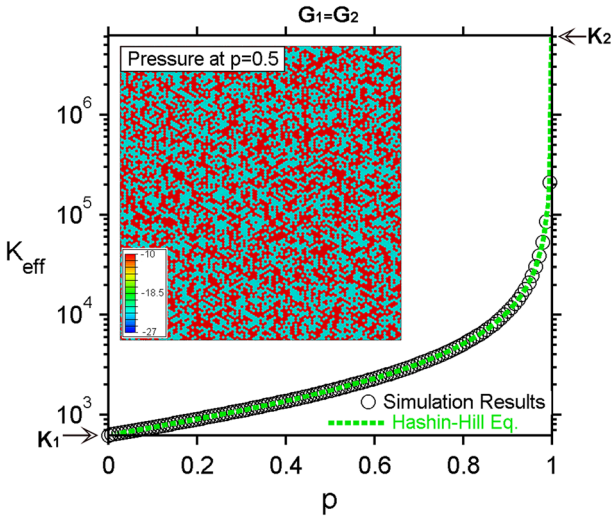

Fig. 2 (Color online) The effective bulk modulus K_{eff} of composite materials comprised of two phases with the same shear moduli ($G_1 = G_2 = 5 \times 10^2$) but different bulk moduli ($K_1 = 6.25 \times 10^2$ and $K_2 = 6.25 \times 10^6$) as a function of phase fraction p. The *black circles* represent simulation results, which are in excellent agreement with predictions of the Hashin–Hill equation [Eq. (10)] drawn as the *green dashed line*. The pressure distribution at $p = 0.5$ shown as the *inset* is consistent with Hill's theory that proposed piecewise pressure (or volumetric strain) when $G_1 = G_2$.

show that with increasing p, percolative shear stress paths emerge and grow, suggesting that shearing in materials is topology-dependent and that G_{eff} exhibits percolation behavior. At low p, there is some localized shear stress concentration. At high p, percolating paths form, involving regions under both positive and negative high shear stresses because of deformation compatibility.

We turn now to the opposite case where the two phases have the same shear moduli but different bulk moduli. The effective bulk modulus K_{eff} as a function of p is plotted in Fig. 2. The Hashin bounds for K_{eff} [31] are

$$K^{(-)} = K_1 + \frac{p}{\frac{1}{K_2 - K_1} + \frac{1-p}{K_1 + G_1}} \tag{8}$$

$$K^{(+)} = K_2 + \frac{1-p}{\frac{1}{K_1 - K_2} + \frac{p}{K_2 + G_2}} \tag{9}$$

When $G_1 = G_2 = G$, the lower and upper bounds coincide ($K^{(-)} = K^{(+)}$), and K_{eff} can be calculated exactly from either equation regardless of the phase geometry [31,38–40].

$$K_{eff} = K_1 + \frac{p}{\frac{1}{K_2 - K_1} + \frac{1-p}{K_1 + G}} = K_2 + \frac{1-p}{\frac{1}{K_1 - K_2} + \frac{p}{K_2 + G}} \tag{10}$$

Our simulation results agree with predictions from Eq. (10) in the entire range of p as shown in Fig. 2. The curve shape resembles a lower bound, which has a percolation threshold at unity and therefore never percolates. K_{eff} does not exhibit intrinsic percolation. This is a very suggestive result, implying that volume change in materials (as modulated by the bulk modulus) is intrinsically independent of topology. Equation (10) being applicable to any phase geometry corroborates this hypothesis.

Hill [38,39] proposed that a sufficient condition for Eq. (10) to be true is to have piecewise constant volumetric strain (or pressure) in each phase. If the volumetric strains are e_1 and e_2 in the two phases respectively, and the pressures are P_1 and P_2, then

$$K_{eff} = \frac{f_1 P_1 + f_2 P_2}{f_1 e_1 + f_2 e_2} = \frac{f_1 K_1 e_1 + f_2 K_2 e_2}{f_1 e_1 + f_2 e_2} \tag{11}$$

An equivalence between Eqs. (10) and (11) would require that $e_1/e_2 = (K_2 + G)/(K_1 + G)$ or $P_1/P_2=[K_1(K_2 + G)]/[K_2(K_1 + G)]$, which renders the displacements and normal tractions continuous at phase boundaries and also satisfies the equilibrium and compatibility requirements. The pressure in our simulations is indeed piecewise constant (e.g., see the inset in Fig. 2), although the individual stress components are not. Also, although the shear moduli of the two phases are the same, the shear stress is not uniform in the material (not shown).

Now we move on to the more general case where the two phases have different bulk and shear moduli. We first examine the effects of the phase bulk moduli contrast, K_2/K_1, on both G_{eff} and K_{eff} by gradually decreasing K_1 while fixing K_2, G_1, and G_2 ($G_2/G_1 = 10^4$). Shown in Fig. 3 are the predicted G_{eff} in (a) and K_{eff} in (b) for $K_2/K_1 = 1, 10, 10^2, 10^3$, and 10^4. In Fig. 3a, G_{eff} decreases with decreasing K_1, subtly and nonlinearly; G_{eff} values for $K_2/K_1 = 10^2$ and 10^3 (blue and green data points) do not always lie in between those for $K_2/K_1 = 1$ and 10^4, but rather coincide with the data for $K_2/K_1 = 1$ at low p and with the data for $K_2/K_1 = 10^4$ at high p. The values of the percolation threshold p_c are evaluated from the percolation probability Π as shown in the bottom right inset, and are assembled in the top left inset in Fig. 3a, together with the scaling exponents s and t from fitting G_{eff} to Eq. (7) on the range $|p - p_c| \leq 0.12$. With increasing K_2/K_1, p_c increases from ~0.503 to 0.558. s and t values for all K_2/K_1 contrasts are within the range of 1.3 ± 0.11 (except for $s = 1.48$ at $K_2/K_1 =10^4$), which presents a similarity with the universality class of conductivity problems. Furthermore, the effect of K_2/K_1 on G_{eff} resembles that of short-range correlations [34], which cause a small shift in the percolation threshold but do not alter scaling. We further run a second set of simulations where $G_2/G_1 = 1.1 \times 10^6$ is much higher and observe the same trend in the increase in p_c as K_2/K_1 is increased from 30 to 3×10^5 (data not shown). With an extremely high K_2/K_1 (relative to G_2/G_1), however, the effect of phase bulk moduli may become very significant and scaling behavior may change. In Fig. 3b, with decreasing K_1 (increasing K_2/K_1), K_{eff} curves shift downward in the low p range while preserving the overall curve shape. These curves for K_{eff} all show percolation features, although more evident at higher K_2/K_1. As K_{eff} in the case of equal shear moduli ($G_1 = G_2$) shown in Fig. 2 does not percolate, we suggest that the apparently *extrinsic* percolation in K_{eff} seen in Fig. 3b originates from the *intrinsic* percolation in G_{eff} shown in Fig. 3a in the presence of shear moduli contrast ($G_2/G_1 = 10^4$).

Figure 4 shows the effect of the phase shear moduli contrast, G_2/G_1, on G_{eff} in (a) and K_{eff} in (b), obtained by gradually increasing G_2 (i.e., increasing G_2/G_1 from 1 to 10^4) while fixing K_1, K_2 and G_1. In Fig. 4a, with increasing G_2, G_{eff} increases in a highly nonlinear fashion, by a larger extent at higher p, but all curves have a shape characteristic of percolation. In Fig. 4b, we observe an increase in K_{eff} as G_2 is increased, especially at high p. Interestingly, there is a drastic change in the curve shape as G_2 increases, from having a single curvature to incurring an inflection in curvature. In particular, the red data points for the case of $G_2/G_1 = 10^4$ show a shape clearly indicating a percolation transition. We again suggest that such transition in the behavior of K_{eff} is extrinsic, and is triggered by the increasing dominance of percolation in G_{eff} at high G_2/G_1 as shown in Fig. 4a.

In light of the above observations, we propose that the Hashin–Hill equation [Eq. (10)], written for the case of two phases having the same shear modulus, may also be profitably

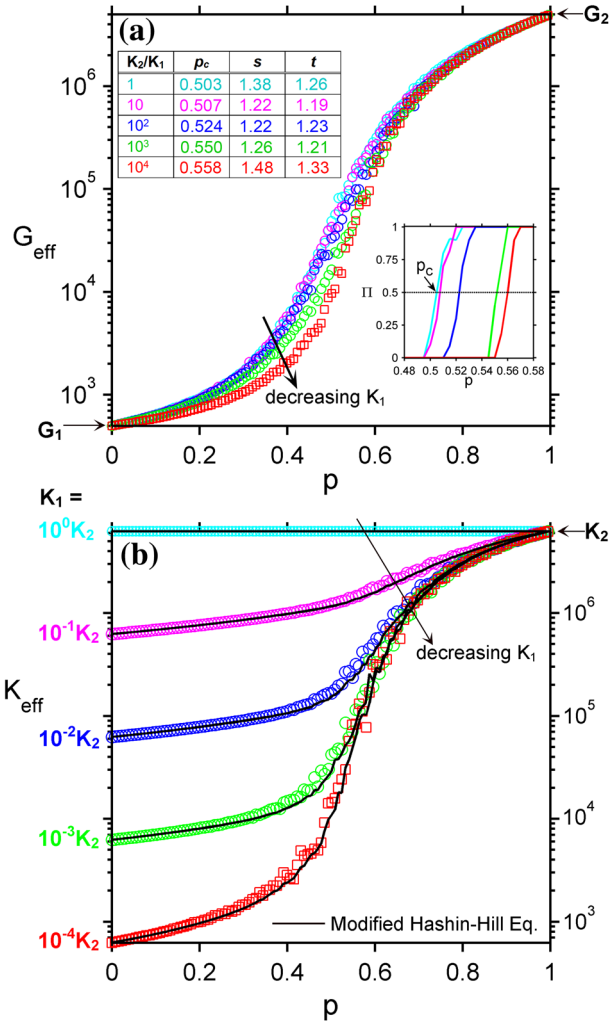

Fig. 3 (Color online) The effective shear modulus G_{eff} (**a**) and effective bulk modulus K_{eff} (**b**) of five families of composite materials with different K_1, while other phase moduli K_2, G_1 and G_2 are all fixed (G_2/G_1 is held at a high contrast of 10^4). In Fig. 3a, the percolation threshold p_c and the scaling exponents s and t extracted from G_{eff} data are assembled in the *top left inset*, and the *bottom right inset* shows how p_c is determined from the percolation probability Π. The *black solid lines* in Fig. 3b are predictions of K_{eff} from the modified Hashin–Hill equation [Eq. (12)].

applied to composites containing phases of different shear moduli, if we replace the common shear modulus by an effective shear modulus. In other words, we hypothesize that Eq. (10) is still applicable when $G_1 \neq G_2$, provided that G in the equation is replaced by G_{eff}.

$$K_{eff} = K_1 + \frac{p}{\frac{1}{K_2-K_1} + \frac{1-p}{K_1+G_{eff}}} = K_2 + \frac{1-p}{\frac{1}{K_1-K_2} + \frac{p}{K_2+G_{eff}}} \tag{12}$$

For the data sets in Figs. 3 and 4, G_{eff} was already obtained from simulations as shown in Figs. 3a and 4a. Using these G_{eff} results, Eq. (12) can predict K_{eff} values, which are

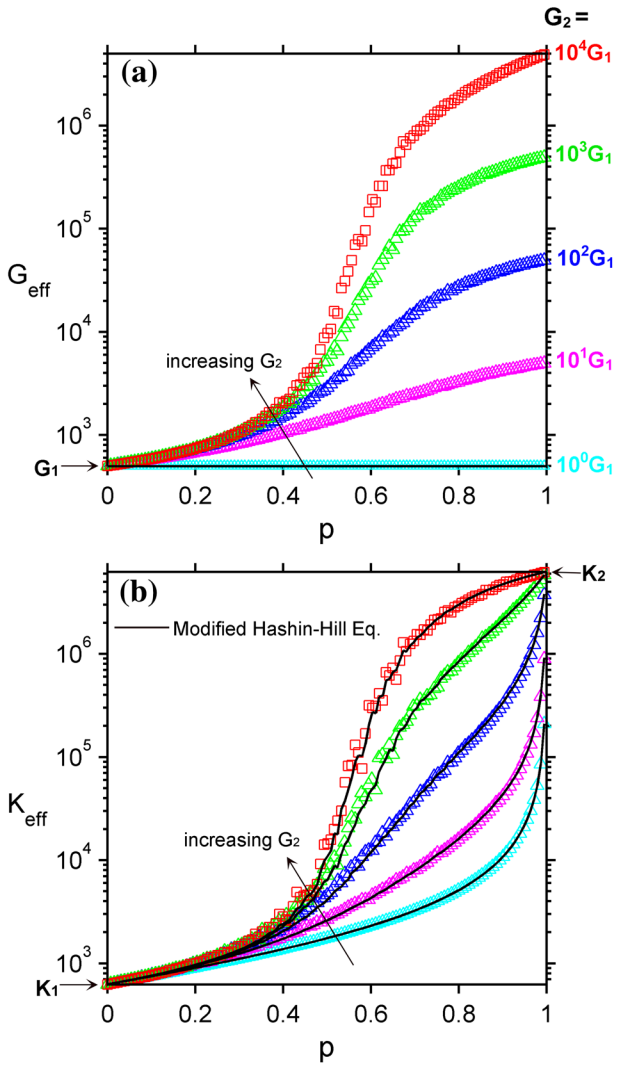

Fig. 4 (Color online) The effective shear modulus G_{eff} (**a**) and effective bulk modulus K_{eff} (**b**) of five families of composite materials with different G_2, while other phase moduli K_1, K_2 and G_1 are all fixed (K_2/K_1 is held at a high contrast of 10^4). The *black solid lines* in (**b**) are predictions of K_{eff} from the modified Hashin–Hill equation [Eq. (12)].

plotted as black solid lines in Figs. 3b and 4b. The predicted K_{eff} is in excellent agreement with K_{eff} obtained from simulations for all curves regardless of whether individual phase bulk or shear moduli are being changed, which is remarkable considering the random phase distribution, high phase contrast, and percolation effects in G_{eff} present in our model system. This discovery thus provides an approximation (rather than a rigorously-derived relation) to predict K_{eff} once G_{eff} is known or can be obtained by other means, by modifying the Hashin–Hill equation to incorporate G_{eff}. Given how wide the rigorous Hashin bounds on K_{eff} are, the ability to accurately predict K_{eff} for arbitrary values of G of the phases should

offer some practical value, and also affirms the utility of introducing percolation concepts into the field of continuum elasticity.

The results shown in Figs. 3b and 4b also support our prior conjecture that percolation in K_{eff} is extrinsic and arises from the intrinsic percolation in G_{eff}. Analytically, G_{eff} may be determined from the GEM equation Eq. (6). Although Eq. (6) does not explicitly incorporate the effect of phase bulk moduli (or K_{eff}) on G_{eff}, it incorporates percolation threshold p_c and scaling exponents s and t that change with phase bulk moduli. The combination of Eqs. (6) and (12) can thus be used to simultaneously predict G_{eff} and K_{eff} for random multiphase materials with a high degree of accuracy.

In summary, while most existing percolation studies deal with scalar properties, we have explored percolation of a typical higher-rank tensor that cannot be reduced to a scalar even for isotropic materials. Assessing the effective bulk and shear moduli, K_{eff} and G_{eff}, of random multiphase materials by a variety of continuum calculations, we showed that G_{eff} exhibits typical, intrinsic, percolation behavior, with scaling exponents similar to those seen in conductivity percolation problems. The percolation threshold for G_{eff}, however, shifts slightly with the contrast in phase bulk moduli. On the contrary, our results suggest that K_{eff} does not exhibit intrinsic percolation. Rather, the cross effects between bulk and shear moduli give rise to what we refer to as "extrinsic percolation" in K_{eff}, originating from the percolation in G_{eff}. This observation allowed us to propose that by incorporating G_{eff} in the Hashin–Hill equation, one can predict K_{eff} even for systems with different phase shear moduli.

Acknowledgments Y. Chen acknowledges the support from RPI start-up fund. C.A.S. acknowledges the support of the U.S. National Science Foundation, under contract CMMI-1332789. Both authors enjoyed the support of the U.S. National Science Foundation under contract DMR-0346848 in the early stages of this work.

References

1. Milton, G.W.: The Theory of Composites. Cambridge University Press, Cambridge (2002)
2. Sahimi, M.: Heterogeneous Materials 1: Linear Transport and Optical Properties. Springer, New York (2003)
3. Kim, I.C., Torquato, S.: Effective conductivity of suspensions of hard spheres by Brownian motion simulation. J. Appl. Phys. **69**, 2280–2289 (1991)
4. Torquato, S.: Random Heterogeneous Materials: Microstructure and Macroscopic Properties. Springer, New York (2002)
5. Choy, T.C.: Effective Medium Theory. Clarendon Press, Oxford (1999)
6. Kantor, Y., Webman, I.: Elastic properties of random percolating systems. Phys. Rev. Lett. **52**, 1891–1894 (1984)
7. Moukarzel, C., Duxbury, P.M.: Stressed backbone and elasticity of random central-force systems. Phys. Rev. Lett **75**, 4055–4058 (1995)
8. Latva-Kokko, M., Timonen, J.: Rigidity of random networks of stiff fibers in the low-density limit. Phys. Rev. E. **64**, 066117 (2001)
9. Zhou, Z.C., Joos, B., Lai, P.Y.: Elasticity of randomly diluted central force networks under tension. Phys. Rev. E. **68**, 055101 (2003)
10. Tighe, B.P., Socolar, J.E.S., Schaeffer, D.G., Mitchener, W.G., Huber, M.L.: Force distributions in a triangular lattice of rigid bars. Phys. Rev. E **72**, 031306 (2005)
11. Jacobs, D.J., Thorpe, M.F.: Generic rigidity percolation: the pebble game. Phys. Rev. Lett. **75**, 4051–4054 (1995)
12. Chen, Y., Schuh, C.A.: Percolation of diffusional creep: a new universality class. Phys. Rev. Lett. **98**, 035701 (2007)
13. Chen, Y., Schuh, C.A.: Coble creep in heterogeneous materials: the role of grain boundary engineering. Phys. Rev. B **76**, 064111 (2007)

14. Drory, A.: Theory of continuum percolation.1. General formalism. Phys. Rev. E **54**, 5992–6002 (1996)
15. Drory, A.: Theory of continuum percolation.2. Mean field theory. Phys. Rev. E **54**, 6003–6013 (1996)
16. Golden, K.M.: Critical behavior of transport in lattice and continuum percolation models. Phys. Rev. Lett. **78**, 3935–3938 (1997)
17. Baker, D.R., Paul, G., Sreenivasan, S., Stanley, H.E.: Continuum percolation threshold for interpenetrating squares and cubes. Phys. Rev. E **66**, 046136 (2002)
18. Hunt, A.G.: Continuum percolation theory for transport properties in porous media. Philos. Mag. **85**, 3409–3434 (2005)
19. Grimaldi, C., Balberg, I.: Tunneling and nonuniversality in continuum percolation systems. Phys. Rev. Lett. **96**, 066602 (2006)
20. Akagawa, S., Odagaki, T.: Geometrical percolation of hard-core ellipsoids of revolution in the continuum. Phys. Rev. E **76**, 051402 (2007)
21. Stevens, D.R., Downen, L.N., Clarke, L.I.: Percolation in nanocomposites with complex geometries: experimental and Monte Carlo simulation studies. Phys. Rev. B **78**, 235425 (2008)
22. Snarskii, A.A., Zhenirovskyy, M.I.: Double-threshold percolation behavior of effective kinetic coefficients. Phys. Rev. E **78**, 021108 (2008)
23. Sangare, D., Adler, P.M.: Continuum percolation of isotropically oriented circular cylinders. Phys. Rev. E **79**, 052101 (2009)
24. Balberg, I., Binenbaum, N., Anderson, C.H.: Critical behavior of the two-dimensional sticks system. Phys. Rev. Lett. **51**, 1605 (1983)
25. Feng, S., Halperin, B.I., Sen, P.N.: Transport properties of continuum systems near the percolation threshold. Phys. Rev. B **35**, 197 (1987)
26. Halperin, B.I., Feng, S., Sen, P.N.: Differences between lattice and continuum percolation transport exponents. Phys. Rev. Lett. **54**, 2391–2394 (1985)
27. Zhu, J., Jabini, A., Golden, K.M., Eicken, H., Morris, M.: A network model for fluid transport through sea ice. Ann. Glaciol. **44**, 129–133 (2006)
28. Chen, Y., Schuh, C.A.: Effective transport properties of random composites: continuum calculations versus mapping to a network. Phys. Rev. E **80**, 040103 (2009)
29. Pecullan, S., Gibiansky, L.V., Torquato, S.: Scale effects on the elastic behavior of periodic and hierarchical two-dimensional composites. J. Mech. Phys. Solids **47**, 1509–1542 (1999)
30. Hazanov, S.: Hill condition and overall properties of composites. Arch. Appl. Mech. **68**, 385–394 (1998)
31. Hashin, Z.: On elastic behaviour of fibre reinforced materials of arbitrary transverse phase geometry. J. Mech. Phys. Solids **13**, 119–134 (1965)
32. Budiansky, B.: On the elastic moduli of some heterogeneous materials. J. Mech. Phys. Solids **13**, 223–227 (1965)
33. Eshelby, J.D.: The determination of the elastic field of an ellipsoidal inclusion, and related problems. Proc. R. Soc. London Ser. A **241**, 376–396 (1957)
34. Chen, Y., Schuh, C.A.: Diffusion on grain boundary networks: percolation theory and effective medium approximations. Acta Mater. **54**, 4709–4720 (2006)
35. McLachlan, D.S., Chiteme, C., Heiss, W.D., Wu, J.J.: Fitting the DC conductivity and first order AC conductivity results for continuum percolation media, using percolation theory and a single phenomenological equation. Physica B **338**, 261–265 (2003)
36. Stauffer, D., Aharony, A.: Introduction to Percolation Theory. Taylor & Francis, London (1992)
37. Clerc, J.P., Giraud, G., Laugier, J.M., Luck, J.M.: The electrical conductivity of binary disordered systems, percolation clusters, fractals and related models. Adv. Phys. **39**, 191–309 (1990)
38. Hill, R.: Theory of mechanical properties of fibre-strengthened materials: I. Elastic behaviour. J. Mech. Phys. Solids **12**, 199–212 (1964)
39. Hill, R.: Elastic properties of reinforced solids: some theoretical principles. J. Mech. Phys. Solids **11**, 357–372 (1963)
40. Thorpe, M.F., Jasiuk, I.: New results in the theory of elasticity for two-dimensional composites. Proc. R. Soc. London Ser. A **438**, 531–544 (1992)